nzsee
NEW ZEALAND SOCIETY FOR EARTHQUAKE ENGINEERING

Seismic strengthening of RC walls using FRP to prevent axial failure

Z. Li, E. del Rey Castillo & R.S. Henry
Department of Civil and Environmental Engineering, University of Auckland, Auckland, New Zealand

ABSTRACT

Reinforced concrete (RC) walls with insufficient compressive strain capacity at the boundary region are vulnerable to premature axial failure, limiting the drift capacity. A solution to strengthen these deficient RC walls by preventing the axial failure was tested using fibre reinforced polymer (FRP) laminates and spike anchors. 75 concrete prisms simulating the wall boundary region were tested using monotonic axial compression loading. A total of 22 different confinement configurations were tested, with the variables being the anchor spacing, prism cross-sectional aspect ratio and anchor cross-sectional area. The maximum compressive strain was about 5 times that of the unconfined prism, achieved when anchor spacing was 90 mm. Subsequently, selected confinement configurations were used to strengthen and investigate three full-scale pre-1970s singly reinforced walls, and the test results were compared with that of another identical wall previously tested by T. Zhang (2019). All walls were with dimension of 150 mm×1920 mm×3840 mm using 10% axial load and tested consistently using axial load and reversed cyclic static loading. The axial failure was shifted to tension-controlled failure by gradual rebar fracture, and the drift at peak of the strengthened walls was about 2.7 times that of the reference wall.

1 INTRODUCTION

Inadequate confinement of the RC wall compression zone, leading to low compressive strain capacity and axial failure, was found to be a seismic deficiency during the Canterbury Earthquakes (Kam et al. 2011; NZSEE 2017). The behaviour of pre-1970s singly reinforced walls was experimentally assessed, which failed by concrete crushing, followed by axial failure and collapse in 2.0% drift when subjected to 10% axial load ratio (Zhang et al. 2018; Zhang 2019). Providing confinement to the wall boundary regions using FRP laminate and spike anchors shown in Figure 1 was considered a solution to this deficiency. An FRP spike anchor is made of a bundle of dry fibres (del Rey Castillo et al. 2019) cured using epoxy resin, with the anchor dowels being installed inside the concrete and anchor fans bonded onto the concrete surface. The design of FRP spike anchors is not part of the scope of current codes or guidelines such as ACI 440 (ACI 2017). To fill this knowledge gap, Li et al tested 75 concrete prisms confined by FRP laminate and spike anchors simulating the confined wall boundary regions using monotonic axial compression testing, with some test results available in a previously published paper (Li et al. 2022). Following on this prisms testing, three pre-1970s unconfined singly reinforced walls based on the research on as-built walls by Zhang were strengthened using FRP laminate and spike anchors to confine the boundary regions, and tested subjected to 10% axial load ratio. The test results of the prisms and walls is presented in this paper, as the fundamental study for developing a design method in the future.

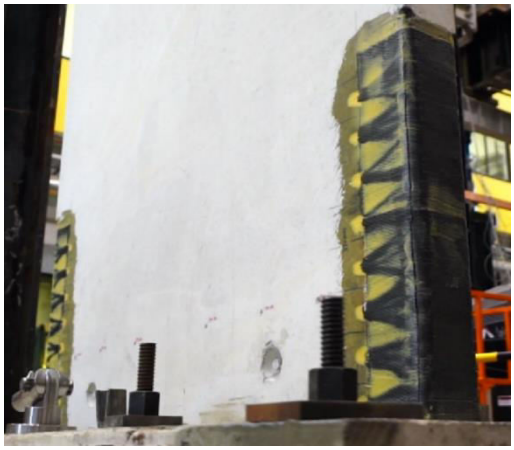

Figure 1 FRP confinement for wall boundary regions

2 EXPERIMENTAL PROGRAM

A series of 75 plain concrete prisms were tested using monotonic axial compression. The prisms were sorted into type A and B, depending on the confinement configuration. Type A used U-shape FRP laminates and spike anchors on only one side, as shown in Figure 2(a), while type B incorporated only FRP spike anchors without U-shape laminates, as shown in Figure 2(b). The geometric parameters included prism width (b), prism length (l), prism height (H), anchor spacing (S_d), cross-sectional area of dry anchor product (A_d), fan length (L_f) and fan with (W_f). The prism width (b) and height (H) was chosen consistently as 150 mm and 360 mm, respectively. The prism length (l), anchor spacing (S_d) and cross-sectional area of dry anchor product (A_d) were the variables investigated, with the range being l=150 mm and 200 mm, S_d=90 mm, 120 mm and 180 mm and A_d=14 mm^2, 28 mm^2 and 56 mm^2, respectively, as summarized in Table 1. The corners wrapped by the FRP were rounded with radius of 28 mm to reduce the influence of stress concentration, so L_f=l-28 mm. All prisms were sorted into 26 groups by different confinement configurations, with the group IDs given in Table 1.

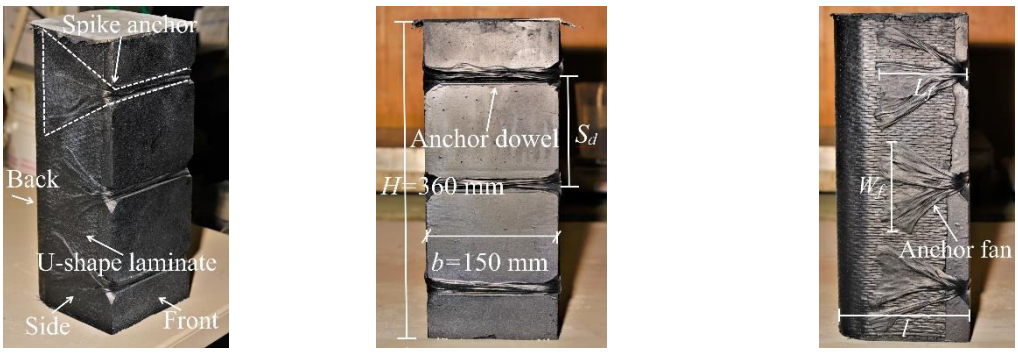

(a)

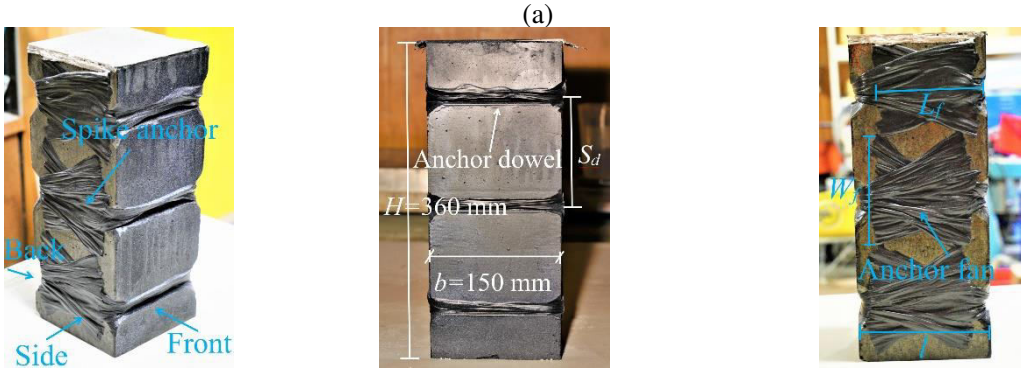

(b)

Figure 2 Test FRP confinement: (a) Type A; (b) Type B

Table 1 Prism test matrix

Confinement type	Confinement ID	l (mm)	L_f (mm)	W_f (mm)	S_d (mm)	A_d (mm^2)
A	S					
	S90-14	150	122	90	90	14
	S120-14		122	120	120	14
	S180-14		122	180	180	14
	S90-28		122	90	90	28
	S120-28		122	120	120	28
	S120-56		122	120	120	28
	S180-28		122	180	180	28
	S180-56		122	180	180	56
	R					
	R90-14	200	172	90	90	14
	R120-14		172	120	120	14
	R180-14		172	180	180	14
	R90-28		172	90	90	28
	R120-28		172	120	120	28
	R120-56		172	120	120	56
	R180-28		172	180	180	28
	R180-56		172	180	180	56
B	DS					
	DS90-28	150	122	90	90	28
	DS120-28		122	120	120	28
	DS180-28		122	180	180	28
	DR					
	DR90-28	200	172	90	90	28
	DR120-28		172	120	120	28
	DR180-28		172	180	180	28

Subsequently, four identical full-scale pre-1970s singly RC walls were tested, with the test matrix being summarized in Table 2. One of them serving as the reference wall SW150-10 (wall ID) was tested previously by Zhang et al (2018; 2019), subjected to 10% axial load ratio and cyclic etc etc. The detailing of the walls is plotted in Figure 3. The dimension of the wall panel was 150 (wall thickness) ×1920 (wall length) × 3840 (wall height) mm×mm×mm. The reinforcement is one layer of horizontal and vertical Grade300E rebars center-to-center spaced at 228 mm with yield strength specified of 300 MPa in accordance with AS/NZS 4671:2001 (2001). The vertical rebars within the boundary region were D16 while the horizontal rebars were D10. The horizontal bars were 90 degrees hooked and the hooks were diagonal to the vertical bars to restrain the vertical D16 rebars from in-plane buckling. The clear cover at the end of the wall to the surface of the hook was 30 mm. The other three walls serving as the strengthened walls were confined with FRP in different configurations, as shown in Figure 3. The wall IDs were the same as the reference wall plus a suffix Greek letter α, β or γ representing different FRP confinement solutions. The confinement configurations used for each solution were different, using at least one of S90-28, R90-28 and R180-56 (confinement ID) as confinement type A or DS90-28 (confinement ID) as confinement type B. The corners of the walls wrapped by the FRP laminate or spike anchors were rounded with a radius of 28 mm. The material properties of the test specimens are summarized in Table 3. Concrete compressive strength was tested according to New Zealand standard NZS3112.2 (1986). Vertical rebar yield strength was tested in accordance with ASTM A370-17 (2017). The FRP elastic modulus and strain of rupture was tested following ASTM D3039 (2017).

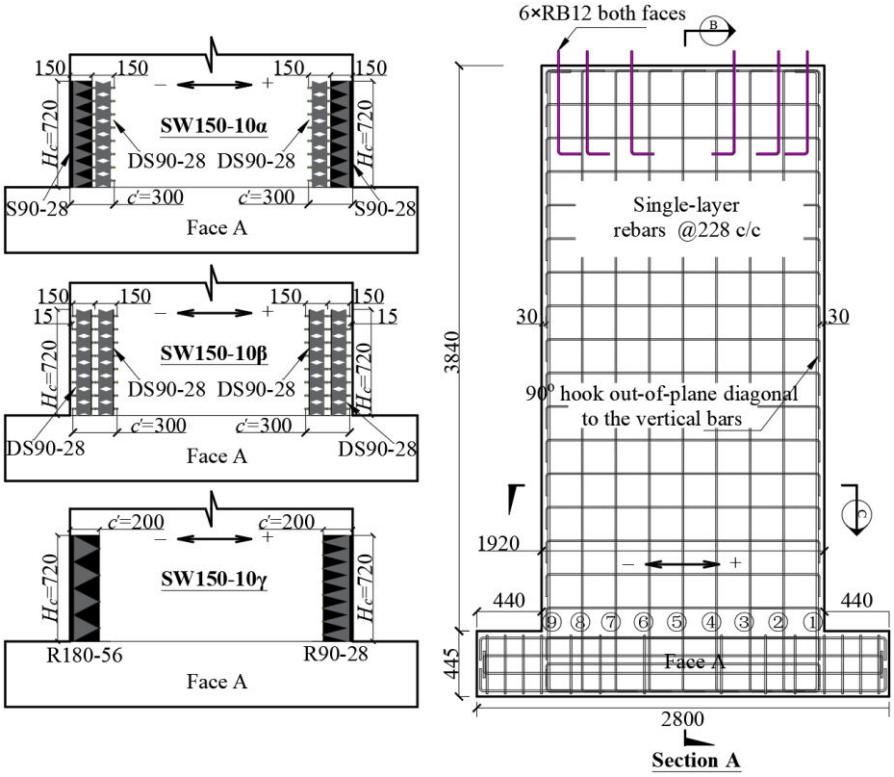

Figure 3 Wall detailing and strengthening design

Table 2 Wall test matrix

Wall ID	Confinement configuration	
	Negative end (-)	Positive end (+)
SW150-10		
SW150-10α	S90-28 and DS90-28	DS90-28 and S90-28
SW150-10β	Dual DS90-28	Dual DS90-28
SW150-10γ	R180-56	R90-28

Table 3 Material properties

Specimen	Concrete strength (MPa)	Vertical bar yield strength (MPa)		FRP laminate		FRP anchor	
		D10	D16	Elastic modulus (GPa)	Strain of rupture (10^{-3})	Elastic modulus (GPa)	Strain of rupture (10^{-3})
Type A prism	29.7			234.4	11.0	236.4	11.8
Type B prism	36.7			234.4	11.0	236.4	11.8
SW150-10	35.3	286.6	294.7	234.4	11.0	236.4	11.8
SW150-10α	36.2	338.2	301.6	234.4	11.0	236.4	11.8
SW150-10β	37.8	338.2	301.6	234.4	11.0	236.4	11.8
SW150-10γ	42.4	338.2	301.6	234.4	11.0	236.4	11.8

The loading test of the prisms was conducted using the 2000 kN compressor shown in Figure 4(a) at a rate of about 0.02 mm per second. Three industrial cameras were used facing the concrete surface perpendicularly towards three sides of the prisms, as shown in Figure 4(a). The photos were taken by these cameras synchronously at set intervals and were computed for the deformation of concrete and FRP using digital image correlation (DIC). The walls were tested using lateral reversed cyclic loadings and constant axial load with axial load ratio of 10%. The loading setup of the walls included five main parts, namely the safety frame, the foundation block pair, the

loading beam, the axial load system and the actuator, as illustrated in Figure 4(b). The protocol of the lateral cyclic loading was determined as displacement-controlled model with 0.005%, 0.01% and 0.075 % 0.15%, 0.20%, 0.25%, 0.35%, 0.50%, 0.75%, 1.0%, 1.5%, 2.0%, 3.0% and 4.5% wall drift levels in order, following ACI ITG-5.1-07 (2007). The instrumentation mainly includes DIC system with five cameras shown in Figure 4(c) and linear pot gauges shown in Figure 4(d), measuring the strain field or deformation of the sections near the foundation.

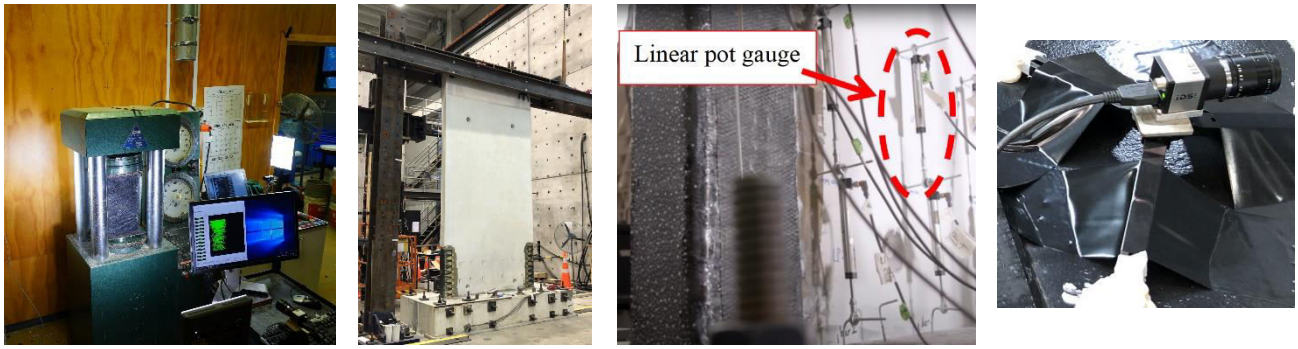

(a) (b) (c) (d)

Figure 4 Loading device: (a) 2000 kN compressor for prisms; (b) Loading frame for walls; (c) Linear pot gauges for walls; (d) DIC camera for walls

3 PRISM TEST RESULTS

The unconfined prisms exhibited diagonal cracking at peak load as shown in Figure 5(a), with the crack propagating until the residual load of 85% of the peak load was reached, which was defined as the failure point. The confined prisms experienced mainly two failure modes depending on the confinement configuration. One was controlled by fibre rupture in the fan, near the key portion where the dowel and the fan meet (fibre rupture), as shown in Figure 5(b). The other one was concrete-controlled failure. Some prisms within this mode experienced concrete spalling at a residual load of about 60% of the peak load, shown in Figure 5(c), including those in the groups of S120-56, S180-56, R120-56 and R180-56. The other prisms failing in this mode exhibited similar damage as the unconfined prisms, with cracks propagating diagonally at a residual load of about 60% of the peak load shown in Figure 5(d). These prisms were in groups of DS180-28 and DR180-28, and no further damage was found at the end of the testing at a residual load of about 50% of the peak load. Therefore, the failure of these prisms was defined at the residual load equal to about 85% of the peak load for the stress-strain curves presented below, consistently with the unconfined prisms. Concrete-controlled failure was observed in the prisms whose S_d, A_d or *l*/*b* were relatively large, while the fibre rupture was observed in the others.

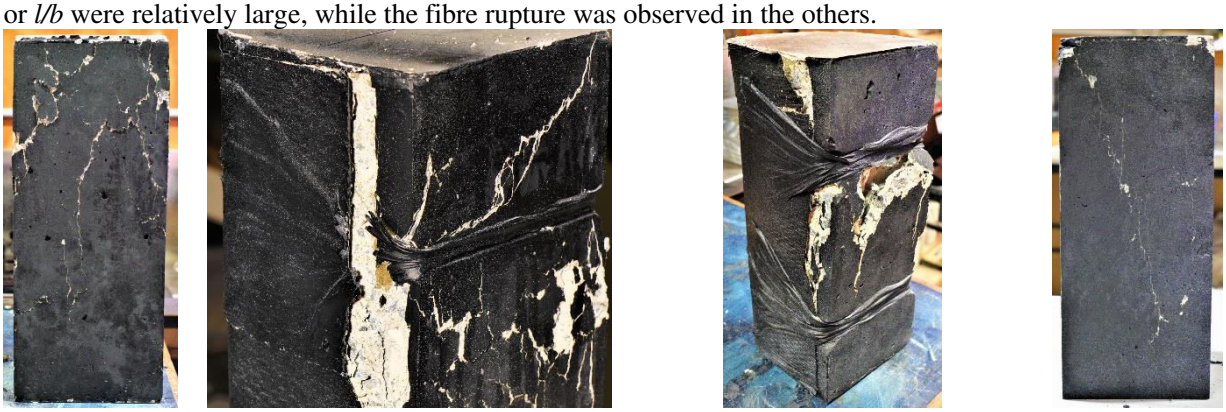

(a) (b) (c) (d)

Figure 5 Commonly observed failure modes: (a) propagated cracks of the unconfined prism (b) fibre rupture; (c) concrete-controlled failure with spalling; (d) concrete-controlled failure without concrete

spalling or damaged in FRP observed

The stress-strain curves of the tested prisms were obtained using DIC and the curves of one prism per group are plotted in Figure 6, with the curves terminating at the failure point as defined above (85% of peak load). For prisms with confinement type A, the strain at failure (ε_{ccu}) increased as the anchor spacing decreased, as illustrated in Figure 6(a) comparing S, S90-28 and S180-28. The largest improvement was observed in the prism in S90-28 with S_d=90 mm, whose ε_{ccu}=0.014, about 4 times as the one of the strain ε_{ccu}=0.0035 from the unconfined prism. A similar effect was observed in the prisms with confinement type B, as shown in Figure 6(b) comparing DS, DS90-28, DS180-28. The largest confined strain ε_{ccu}=0.0154 measured in prism DS90-28 was about 5 times the unconfined strain of ε_{ccu}=0.0031 measured in prism DS. The stress-strasin behavior was compared between confinements consistent in the amount of fiber used but in different configurations, as plotted in Figure 6(c) comparing S90-28 and R180-56. The anchor spacing of R180-56 was double that of S90-28 while the anchor cross-sectional area of A_d was double as well, so that the gross cross-sectional area of the dry anchor dowels is consistent as 112 mm^2. The peak strength of R180-56 was about 1.3 time that of S90-28, and the failure strains were similar, but the post-peak branch of R180-56 was significantly shaper than that of S90-28, because R180-56 and S90-28 ended up with 32.1 kN and 27.5 kN, respectively, with only 14.3% difference. More test results is available in a previously published paper (Li et al. 2022).

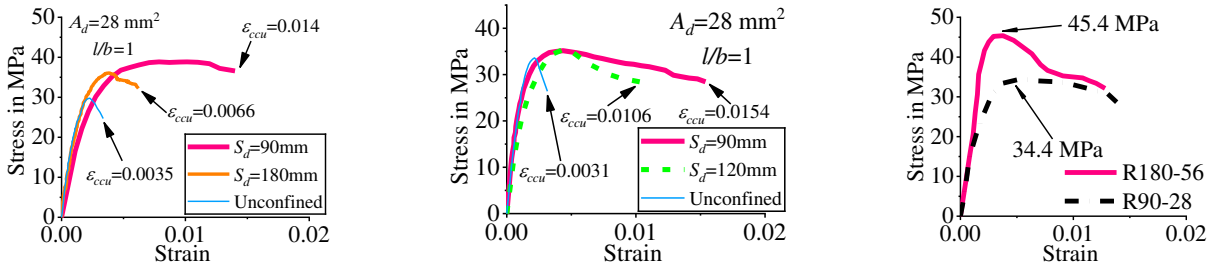

Figure 6 Tested stress-strain responses of the prisms: (a) effect of anchor spacing (Type A); (b) effect of anchor spacing (Type B); (c) comparing R180-56 and S90-28

4 WALL TEST RESULTS

It should be noted that all test results of SW150-10 in this section are from a previous study (Zhang et al. 2018; Zhang 2019). The improvement of the FRP confined wall boundary regions in compressive strain capacity enhanced the wall drift capacity while reducing the concrete damage of the 1970s singly reinforced walls. The reference wall experienced axial failure shown in Figure 7(a) with the entire plastic region crushing and collapsing in the cycle of 2.0% drift. By contrast, only cracking or light spalling was observed on the strengthened walls at 3.0% drift, with SW150-10α shown in Figure 7(b). The crack maps of SW150-10 and SW150-10α are compared using Figure 7(c and d). The FRP confinement of the boundary regions not only increased the number of the cracks but also extended the cracking propagation. The cracking ended at 1.0% drift in the reference wall due to premature axial failure, while extending to 2.0% drift in the strengthened ones. The bottom crack had not reached mid-length in the reference wall, but had gone over the mid-length in the strengthened walls.

(a) (b)

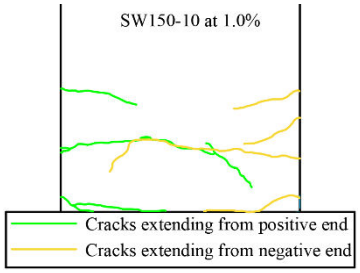

(c)

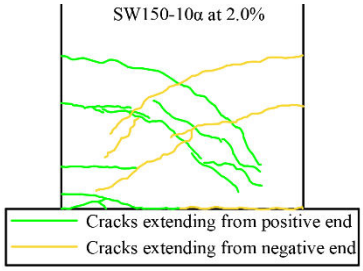

(d)

Figure 7 Wall damage status: (a) SW150-10 at 2.0% drift; (b) SW150-10α at 3.0% drift; (c) crack map of SW150-10; (d) crack map of SW150-10α

The backbone curves extracted from the tested hysteresis loops of all walls are shown in Figure 8(a). The reference wall SW150-10 experienced no vertical rebar fracture, and failed in axial failure in 2.0% drift, so the drift capacity was controlled by the concrete behavior. As a result, the maximum load was attained at 0.75% at around 280 kN, and the load dropped drastically down to zero in 2.0% drift. This failure mode was prevented on the strengthened walls, and shifted to tension-controlled failure with all vertical rebars fracturing progressively. In addition to the concrete damage and rebar fracture shown in Figure 8(b), other damage was observed on the strengthened walls, including FRP laminate rupture shown in Figure 8(c) and FRP anchor dowel shown in Figure 8(d). However, the residual capacity of the strengthened wall was governed by the vertical rebar fracture, so this minor damage did not affect the wall behaviour. Following the first rebar fracture, the lateral load capacity decreased gradually down to around 60% of the peak load at up to 3.0% lateral drift, when all rebars had fractured in all strengthened walls. The peak load was reached in a drift of up to 2.0% that is 2.7 times the one of the reference wall, which indicates that the FRP confinement for the boundary regions can improve the drift capacity of the walls.

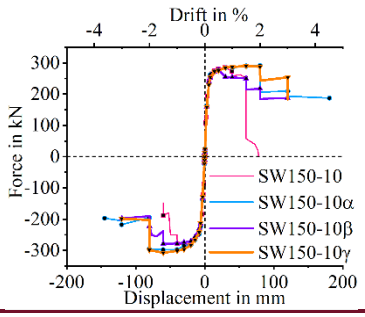

(a)

(b)

(c)

(d)

Figure 8 Backbone curves and test observations: (a) backbone curves; (b) vertical rebar fracture; (c) FRP laminate rupture; (d) FRP dowel rupture

5 CONCLUSIONS

A total 75 concrete prisms and four walls (including one reference wall and three strengthened walls) were tested to understand the behavior of the wall with boundary regions confined with FRP. The stress-strain behavior of the confined prisms and the load-displacement responses of the walls were presented, as well as the test observations, the cracking behavior and load-displacement responses of the walls. Key conclusions are given below:

- The failure strain of the concrete prisms after being confined was multiplied up to about 5 times when the anchor spacing was 90 mm;
- The reference wall experienced axial failure at 2.0% drift, but only cracking or light spalling was observed as the main damage of the strengthened walls at 3.0% drift;
- The cracking ended at 1.0% drift in the reference wall due to premature axial failure, while extending to 2.0% drift in the strengthened ones;
- With FRP confinement, the axial failure of was changed into tension-controlled failure, and the drift at peak of the strengthened walls was improved to up to about 2.7 times that of the reference wall.

6 ACKNOWLEDGEMENT

Research funding was supported by Earthquake Commission (EQC), Mapei New Zealand and the University of Auckland. The authors would like to thank Allied Concrete NZ for providing the ready-mix concrete and Mapei New Zealand and Sika New Zealand for providing the FRP products and epoxy resin products. The generous technical support from BBR Contech in the installation of the FRP materials is appreciated.

7 REFERENCES

Abdullah, S. A., and Wallace, J. W. 2021. "Drift capacity at axial failure of RC structural walls and wall piers." *Journal of Structural Engineering*, 147(6), 04021062.

ACI (American Concrete Institute). 2007. "*Acceptance criteria for specialunbonded post-tensioned precast structural walls based on validationtesting and commentary*." ACI ITG-5.1-07. Detroit.

ACI (American Concrete Institute). 2017. "*Guide for the Design and Construction of Externally Bonded FRP Systems for Strengthening Concrete Structures*." ACI 440.2R. Farming Hills, Michigan, U.S.A.

AS (Standards Australia) and NZS (Standards New Zealand). 2001. "*Steel reinforcing materials*." AS/NZS 4671. Sydney, Australia and Wellington, New Zealand.

ASTM (American Society for Testing and Materials). 2017. "*Standard Test Method for Tensile Properties of Polymer Matrix Composite Materials*." ASTM D3039. West Conshohocken, Pennsylvania.

del Rey Castillo, E., Dizhur, D., Griffith, M., and Ingham, J. 2019. "Strengthening RC structures using FRP spike anchors in combination with EBR systems." *Composite Structures*, 209, 668-685.

ASTM (American Society for Testing and Materials). 2017. "*Standard Test Methods and Definitions for Mechanical Testing of Steel Products: American Society for Testing and Materials*." ASTM A370-17. 100 Barr Harbor Drive, PO Box C700, West Conshohocken, PA 19428-2959. United States.

Kam, W. Y., Pampanin, S., and Elwood, K. 2011. "Seismic performance of reinforced concrete buildings in the 22 February Christchurch (Lyttelton) earthquake." *Bulletin of the New Zealand society for earthquake engineering*, 44(4), 239-278.

Li, Z., del Rey Castillo, E., Henry, R. S., and Thompson, A. 2022. "Axial Behavior of Concrete Prisms Confined by FRP Laminate and Spike Anchors." *Journal of Composites for Construction*, 26(1), 04021058.

NZS (New Zealand Standards). 1986. "*Methods of test for concrete – Tests relating to the determination of strength of concrete*." NZS 3112.2. Wellington.

NZS (New Zealand Standards). 2006. "*Concrete structures standard*." NZS 3101. Wellington, New Zealand.

NZ Red Book. 2017. "*The Seismic Assessment of Existing Buildings*." NZSEE.

Zhang, T. 2019. "Seismic Assessment of Reinforced Concrete Walls in Pre-1970s Multi-Storey Buildings." Ph.D. thesis, University of Auckland, Auckland, New Zealand.

Zhang, T., Elwood, K., and Henry, R. 2018 "Testing of singly reinforced concrete walls used in existing buildings." *Proc., 2018 NZSEE Annual Conference*, 1-8.